

Faculty of Engineering
Faculty of Engineering - Papers

University of Wollongong

Year 2002

Calculation of the hysteretic force
between a superconductor and a magnet

M. J. Qin* G. Li† H. K. Liu‡
S. X. Dou** E. H. Brandt††

*University of Wollongong

†University of Wollongong

‡University of Wollongong, hua@uow.edu.au

**University of Wollongong, shi@uow.edu.au

††Max-Planck Institut fur Metallforschung, Germany

This article was originally published as: Qin, MJ, Li, G, Liu, HK, Dou, SX & Brandt, EH, Calculation of the hysteretic force between a superconductor and a magnet, Physical Review B, 2002, 66, 024516. Copyright 2002 American Physical Society. The original journal can be found here.

This paper is posted at Research Online.

<http://ro.uow.edu.au/engpapers/237>

Calculation of the hysteretic force between a superconductor and a magnet

M. J. Qin, G. Li, H. K. Liu, and S. X. Dou

Institute for Superconducting and Electronic Materials, University of Wollongong, Wollongong NSW 2522, Australia

E. H. Brandt

Max-Planck-Institut für Metallforschung, Institut für Physik, D-70506 Stuttgart, Germany

(Received 19 November 2001; published 17 July 2002)

The magnetic levitation forces exerted on a high-temperature superconducting (HTS) disk by a cylindrical permanent magnet (PM) are calculated from first principles for superconductors with finite thickness. The current $j(\rho, z)$ and field $B(\rho, z)$ profiles in the HTS in the nonuniform magnetic field generated by the PM are derived. The levitation force depends nonlinearly on the critical current density j_c and on the thickness of the HTS. The flux creep is described by a current-voltage law $E(j) = E_c(j/j_c)^n$, from which we show that the levitation force depends on the speed at which the PM approaches or recedes from the HTS, which accounts for the experimentally observed force creep phenomenon. The stiffness of the system is derived by calculating minor force loops. The numerical results reproduce many of the features observed in experiments.

DOI: 10.1103/PhysRevB.66.024516

PACS number(s): 74.60.-w, 74.25.Ha, 74.25.Ld

I. INTRODUCTION

It has been well known that a permanent magnet (PM) can be stably levitated above a high-temperature superconductor (HTS) cooled by liquid nitrogen, which has become the well-known symbol for HTS technology. This fascinating magnetic levitation results from the interaction of the induced current inside the superconductor with the inhomogeneous magnetic field generated by the PM. Because of its possible industrial applications, such as noncontacted superconducting bearings,^{1,2} gravimeters,³ flywheel energy storage systems,⁴⁻⁹ magnetic levitation transport systems,¹⁰ and motors,¹¹ the magnetic levitation between a PM and an HTS has been the subject of intensive studies for the last decade.

The most common feature of the magnetic levitation is the hysteretic behavior of the vertical force F_z versus the distance z between the PM and the HTS when the PM is descending to and then ascending from the HTS. When a PM approaches a zero-field-cooled HTS, the levitation force increases monotonically from zero; as the PM is moving away from the HTS, the levitation force decreases sharply to a negative peak at some distance, indicating attractive force between the HTS and the PM, then declines to zero again at larger distance. Detailed experiments have been performed on melt-textured-grown (MTG) YBCO and RBCO (R denotes a rare earth element such as Nd, Sm, Gd, Eu, Dy, Ho, Er, Tm, Yb, Lu, and La), thin films, as well as granular samples.^{4,12-16} For MTG YBCO and RBCO samples, the force curve is usually asymmetrical, i.e., the absolute value of the attractive force is smaller than the maximum repulsive force $|F_{a,max}| < F_{r,max}$.¹⁶ For thin films, the force curve is almost symmetrical $|F_{a,max}| \approx F_{r,max}$,¹⁷ while for granular samples, the attractive force is hardly present.¹⁸

Various parameters are very important in determining the levitation force. The most important are the pinning strength (critical current density) of the HTS and the induced shielding current loops inside the HTS. Higher j_c and larger loops are very important to achieve a high levitation force. It has been suggested that the levitation force increases linearly

with j_c and more than linearly with the size of the current loops.¹³ According to this criterion, the current material of choice for superconducting levitation is MTG YBCO and RBCO samples, because high quality MTG samples with high critical current density and single domain diameters up to 10 cm are currently available by means of the melt process.¹⁹ Another reason is its high irreversibility line at liquid nitrogen temperature, which is the normal operating temperature for magnetic levitation experiments. Although higher critical current density can be achieved in thin films, the levitation force is limited by the thickness of the films.

According to the critical state model,^{20,21} the levitation force is independent of the speed at which the PM approaches and recedes from the HTS.²² However, as the thermally activated flux motion is prominent in HTS, resulting in the relaxation of the magnetization (current density),²³ the levitation force which depends on the current density of the HTS is expected to decrease with time (force creep). Experimentally the levitation force is observed to be approximately logarithmic in time and can be well correlated with the thermally activated flux motion in HTS.²⁴

The thickness of the HTS also drastically influences the levitation force. Because the critical current density is limited, for thin HTS samples, the levitation force increases linearly with the thickness of the HTS. However, beyond a certain thickness, the levitation force is independent of the thickness.²⁵ Other characteristics of the HTS, such as the anisotropy and the grain orientation inside the MTG samples have been studied and shown to affect the levitation force.^{14,26} The stiffness of the PM-HTS system, which represents the spring constant associated with vibrational motion of the levitation system has been intensively studied. Experimental results for vertical stiffness, lateral stiffness and cross stiffness have been presented.^{4,12}

In addition to these, the geometry and properties of the PM also affect the levitation force. The size and shape of the PM, the homogeneity and the temperature dependence of the PM magnetization have been shown to influence the levitation force.¹²

Although the magnetic levitation of a PM above a HTS, and vice versa, can be easily demonstrated, and detailed experimental results for the levitation force have been presented, the theoretical models for this magnetic levitation system have not been fully developed so far. The first reason is that a correct model should consider the finite thickness of a superconducting disk in a perpendicular magnetic field. In the case of an infinite long cylinder under a parallel applied magnetic field, the magnetic field and current density profiles can be easily obtained by means of the critical state model. However, for a superconducting disk under a perpendicularly applied magnetic field, the extreme demagnetization effects make this case qualitatively different from the parallel field case. The second reason is that the calculation now has to consider the response of a HTS immersed into the nonuniform magnetic field generated by the PM or by any other magnet.

In order to avoid the above difficulties, all the models for the magnetic levitation force presented so far made various assumptions. Most of the models are based on the critical state model,^{20,21} which has long been used to account for the irreversible properties of type-II superconductors. The image model^{27–29} treats the superconductor as an ideal diamagnet and the PM as a set of magnetic dipoles; this model disregards the magnetic hysteresis. The system then reduces to two magnetic dipoles, representing the PM and its mirror image, oppositely magnetized and positioned at the same distance below and above the superconductor surfaces. The advantage of this model is that analytical expressions can be obtained. However, it cannot be used to account for the dynamic stiffness. The extension of the image model to include another “frozen” image of the PM has been introduced to explain the dynamic stiffness of the system.³⁰

In a recent article Navau and Sanchez³¹ reviewed the models based on the critical state. Early models considered only the extreme limits of complete flux exclusion or complete flux penetration; they thus described the behavior of type-I superconductors or type-II superconductors with very high critical current.^{27,32} This model was later extended to describe flux penetration.^{33–35} However, these models assumed a superconducting sample small enough to allow the magnetic field gradient to be considered constant along the sample. At the same time, the demagnetization effects caused by the finite size of the superconductor were disregarded. Navau and Sanchez³¹ have accounted for the demagnetization by introducing a demagnetization factor. However, it should be pointed out that the use of demagnetization factors for superconductors in the mixed state in which current is distributed inside the bulk sample, is qualitatively invalid.^{36,37} Although the authors considered a nonuniform field gradient along the sample, the radial magnetic field generated by the PM has been neglected. In typical experiments, however, the PM is smaller than the HTS, and the assumption that the radial field may be disregarded is not realistic.

The levitation force between a cylindrical magnet and granular superconductors has also been reported.^{39,38} The authors assumed that the grains are in the critical state model with an uniform magnetization M and obtained good agreement between the experimental results and the calculations.

The models mentioned above can be used to account for some features of the levitation force observed in experiments, but, they usually are a crude approximation. First, the current and field distribution in the HTS under a nonuniform magnetic field is not adequately accounted for. For practical applications using magnetic levitation, the precise control of the interacting force between a superconducting target and the applied nonuniform magnetic field is of critical importance. It is hence necessary to thoroughly understand the hysteretic nature of the force on a superconductor immersed in such fields. From an analytical point of view, precise knowledge of current and field profiles is essential for the calculation of the magnetic levitation force between a PM and an HTS. Second, the models are all based on the critical state model, which completely disregards flux-creep effects. However, at nitrogen temperature, which is the typical operating temperature for levitation experiments, flux creep is expected to influence the levitation force. Numerical analysis such as the finite element method (FEM) has been applied to calculate the magnetic levitation force; this approach allows us to derive the current and field profiles inside the HTS, but it neglects flux creep as well.

To better understand the design of the magnetic levitation system between the PM and the HTS, a better model is required. In this paper, we take all the above points into account and develop a model that correctly describes the typical experimental configuration and reproduces the experimentally observed features of the magnetic levitation force. The demagnetization effects are considered by explicitly calculating the current and field profiles and the magnetization of superconductors with finite thickness. The flux creep effect is taken into account by using a current–voltage law $E(J) = E_c(J/J_c)^n$ with creep exponent $n = \sigma + 1 \gg 1$, see below.

The paper is structured as follows, In Sec. II we discuss the theories for both a permanent magnet and a superconductor in a nonuniform magnetic field, explaining the assumptions made and some numerical considerations. The results of the calculations, including the effects of the shape and materials properties of the HTS on the levitation force, the force-creep effects, the minor loops, and the stiffnesses will be presented and compared with published experiments in Sec. III, and Sec. IV gives the concluding remarks.

II. MODELING

A. Field of a permanent magnet

We consider a superconducting disk with radius a and thickness $2b$, levitated over a co-axial cylindrical permanent magnet with radius R_{PM} and thickness t_{PM} . The top surface center of the PM is taken as the origin of the cylindrical coordinate system (ρ, ϕ, z) . Because of the axial symmetry of the system, only the cross section of the system is considered, with the z axis chosen as the symmetry axis of both the HTS and the PM, and ρ (radial direction) parallel to the surfaces of the HTS and the PM. For this configuration, the vector potential of the PM has only one component along the ϕ direction, which can be derived by integrating the vector potential of a circular current loop with radius R_{PM} along the thickness t_{PM} ,

$$A_\phi(\rho, z) = \frac{B_{\text{rem}}}{2\pi} \int_0^\pi R_{\text{PM}} \cos \phi \ln \frac{(z + t_{\text{PM}}) + \sqrt{R_{\text{PM}}^2 + \rho^2 - 2\rho R_{\text{PM}} \cos \phi + (z + t_{\text{PM}})^2}}{z + \sqrt{R_{\text{PM}}^2 + \rho^2 - 2\rho R_{\text{PM}} \cos \phi + z^2}} d\phi, \quad (1)$$

where B_{rem} is the remanent induction of the PM. The radial field $B_\rho = -\partial A_\phi / \partial z$ can then be written as

$$B_\rho(\rho, z) = \frac{B_{\text{rem}}}{\pi} \sqrt{\frac{R_{\text{PM}}}{\rho}} \sum_{i=0}^1 \frac{(-1)^i}{k_i} \left[\left(1 - \frac{1}{2} k_i^2\right) K(k_i) - E(k_i) \right], \quad (2)$$

where K and E are complete elliptic integrals of the first and second kind, respectively. And

$$k_i^2 = \frac{4\rho R_{\text{PM}}}{(R_{\text{PM}} + \rho)^2 + (z + it_{\text{PM}})^2}, \quad i=0,1.$$

The axial field $B_z = (1/\rho) \partial(\rho A_\phi) / \partial \rho$ is

$$B_z(\rho, z) = \frac{B_{\text{PM}}}{2\pi} \int_0^\pi \frac{\rho R_{\text{PM}} \cos \phi - R_{\text{PM}}^2 \cos^2 \phi}{R_{\text{PM}}^2 + \rho^2 - 2\rho R_{\text{PM}} \cos \phi} \times \sum_{i=0}^1 \frac{(-1)^i (z + it_{\text{PM}})}{\sqrt{R_{\text{PM}}^2 + \rho^2 - 2\rho R_{\text{PM}} \cos \phi + (z + it_{\text{PM}})^2}} \times d\phi + \frac{A_\phi}{\rho}. \quad (3)$$

B. Superconducting disk in a nonuniform field

The response of superconducting disks and strips in an uniform applied magnetic field has been extensively studied by Brandt.^{40,41} We now consider the response of a superconducting disk in the nonuniform magnetic field generated by the PM [Eqs. (2) and (3)]. The calculation is for the zero-field-cooled (ZFC) process, in which the superconducting disk is cooled below its critical temperature T_c in zero applied field and then a nonuniform field is applied to the disk, which generates a screening current. The central idea of our numerical method is to find the equation of motion for the current density in the superconductor disk filling the space $-b \leq z \leq b$, $\rho \leq a$.

Because of the axial symmetry, the current density J and the vector potential A_J generated by the current have only one component along the ϕ direction. The total vector potential of the system is then $A = A_J + A_\phi$, and the total magnetic field $\mathbf{B} = \nabla \times \mathbf{A}$. We assume here the material law $\mathbf{B} = \mu_0 \mathbf{H}$, which is a good approximation when the flux density B and the critical sheet current $2bJ_c$ are larger than the lower critical field B_{c1} everywhere in the superconducting disk. This requirement is often satisfied in magnetic levitation measurements, normally operated at a relatively high temperature of 77 K. According to the Maxwell equation with gauge $\nabla \cdot \mathbf{A}_J = 0$, we have $\mu_0 \mathbf{J} = \nabla \times \mathbf{B} = \nabla \times \nabla \times \mathbf{A} = \nabla \times \nabla \times \mathbf{A}_J = -\nabla^2 \mathbf{A}_J$. The solution of this Laplace equation in cylindrical geometry can be written as

$$A_J(\rho, z) = -\mu_0 \int_0^a d\rho' \int_{-b}^b dz' Q(r, r') J(r'), \quad (4)$$

with $r = (\rho, z)$ and $r' = (\rho', z')$. The integral kernel is

$$Q(r, r') = f(\rho, \rho', z - z'), \quad (5)$$

with

$$f(\rho, \rho', \eta) = \frac{-1}{\pi k} \sqrt{\frac{\rho'}{\rho}} \left[\left(1 - \frac{1}{2} k^2\right) K(k) - E(k) \right], \quad (6)$$

$$k^2 = \frac{4\rho\rho'}{(\rho + \rho')^2 + \eta^2},$$

K and E are the complete elliptic integrals of the first and second kind, respectively.

Equation (5) is obtained by integrating the three-dimensional (3D) Green function of the Laplace equation $1/4\pi|r_3 - r'_3|$ with $r_3 = (x, y, z)$, over the angle $\phi = \arctan(y/x)$.⁴¹ The total vector potential can then be written as

$$A(\rho, z) = -\mu_0 \int_0^a d\rho' \int_{-b}^b dz' Q(r, r') J(r') + A_\phi(\rho, z). \quad (7)$$

To obtain the desired equation of motion for the current density $J(\rho, z, t)$, we express the induction law $\nabla \times \mathbf{E} = -\dot{\mathbf{B}} = \nabla \times \dot{\mathbf{A}}$ in the form $\mathbf{E} = -\dot{\mathbf{A}}$, where \mathbf{E} is the local electric field caused by vortex motion. Combining this expression with Eq. (7), we have

$$E(\rho, z) = \mu_0 \int_0^a d\rho' \int_{-b}^b dz' Q(r, r') J(r') - \dot{A}_\phi(\rho, z). \quad (8)$$

The equation of motion for the current density can be derived by inverting Eq. (8) as

$$J(\rho, z) = \frac{1}{\mu_0} \int_0^a d\rho' \int_{-b}^b dz' Q^{-1}(r, r') [E(r, r') + \dot{A}_\phi(\rho', z')], \quad (9)$$

where Q^{-1} is the reciprocal kernel defined by

$$\int_0^a d\rho' \int_{-b}^b dz' Q^{-1}(r, r') Q(r', r'') = \delta(r - r''). \quad (10)$$

It can be seen from Eq. (9) that the equation of motion for the current density contains the reciprocal kernel, which depends only on the geometry of the superconducting sample. Here we consider a disk, but the kernel Q can be changed to

calculate other sample geometries, such as strips, and samples with arbitrary cross section.⁴¹ If desired, a possible B dependence of $J_c(B)$, or any generalized law $E=E(J,B)$ is easily incorporated into these computations. Note that, e.g., in the regime of free flux flow one has $E \propto JB$. Generalizations of this method have also been given which consider nonzero lower critical field B_{c1} (Ref. 42) and nonzero London penetration depth λ .⁴³

Equation (9) depends explicitly (i.e., not via separate boundary conditions) on the applied magnetic field via its vector potential A_ϕ . In this paper we consider the field of a permanent magnet given by Eqs. (2) and (3), but one may also use other types of magnetic field, such as the field generated by a circular current loop or by dipoles. In addition to these, the equation also depends on the material law $E=E(J)$ of the superconducting sample. Obviously any sufficiently sharply bent $E(J)$ law may be used; in the following we choose the rather general material law $E(J)=E_c(J/J_c)^n$, which yields the limits of the critical state model for $n \rightarrow \infty$, the flux flow model for $n=1$, and the flux creep model for $1 < n < \infty$. The current is assumed to flow along the electric field \mathbf{E} , thus this current-voltage law may also be written in the form $\mathbf{E}=\rho_c|J/J_c|^\sigma \mathbf{J}$ with exponent $\sigma=n-1$.

Equation (9) is easily time integrated by starting with $J(\rho,z,t=0)=0$ at time $t=0$ and then putting $J(\rho,z,t=t+dt)=J(\rho,z,t)+\dot{J}(\rho,z,t)dt$. The vector potential can then be derived from Eq. (7) and the magnetic field is $\mathbf{B}=\nabla \times \mathbf{A}$. For all the calculations in this paper, we use reduced units of $B_{\text{rem}}=E_c=a=\mu_0=1$, the current density J is in unit of $B_{\text{rem}}/(\mu_0 a)$, the frequency ω is in unit of $E_c/(B_{\text{rem}} a)$, and the levitation force is in units $B_{\text{rem}}^2 a^2/\mu_0$. For simplicity, the critical current is assumed to be independent of the magnetic field.

C. Levitation force and hysteresis loop

The PM approaches and recedes from the HTS as $z(t)=z_{00}+z_0-z_0 \sin(\omega t)$, where $z_{00}+z_0$ is the maximum (initial) distance and z_{00} the minimum distance between the PM and the HTS ($\omega t=0 \rightarrow \pi/2 \rightarrow \pi$). The frequency ω defines the speed at which the PM approaches and recedes from the HTS. Experimentally, uncertainty will be caused when the PM touches the HTS, and therefore the limit $z_{00}=0$ should be avoided. In this calculation we choose $z_{00}/a=0.1$ as the minimum distance between the PM and the superconducting disk.

After the current density inside the superconducting disk is derived, the vertical levitation force along the z axis can be readily obtained as

$$F_z=2\pi \int_0^a d\rho \int_{-b}^b dz J(\rho,z) B_\rho(\rho,z), \quad (11)$$

where $B_\rho(\rho,z)$ is the radial component of the applied magnetic field, Eq. (2). Note that this radial component, and thus the axial magnetic force, is nonzero only for an inhomogeneous applied field. Actually, the correct magnetic force would also be obtained by inserting in the integral (11) the

total magnetic field, since the self-force exerted by any current distribution on its own magnetic field is zero.

As a measure of the strength of the applied nonuniform field we choose the field value $B_{\text{axis}}=B_z(\rho=0,z)$ occurring at the center of the bottom surface of the superconducting disk

$$B_{\text{axis}}=\frac{B_{\text{rem}}}{2} \left[\frac{z+t_{\text{PM}}}{\sqrt{R_{\text{PM}}^2+(z+t_{\text{PM}})^2}} - \frac{z}{\sqrt{R_{\text{PM}}^2+z^2}} \right]. \quad (12)$$

The magnetic moment of the disk is

$$m=2\pi \int_0^a d\rho \int_{-b}^b dz \rho^2 J(\rho,z). \quad (13)$$

D. Minor force loops and magnetic stiffness

Because of the hysteretic behavior of the superconducting disk, when the PM is moved away and back again by a small amount δz at a distance z , the $F_z(z)$ curve follows a minor force loop rather than the major force loop. For small δz , the

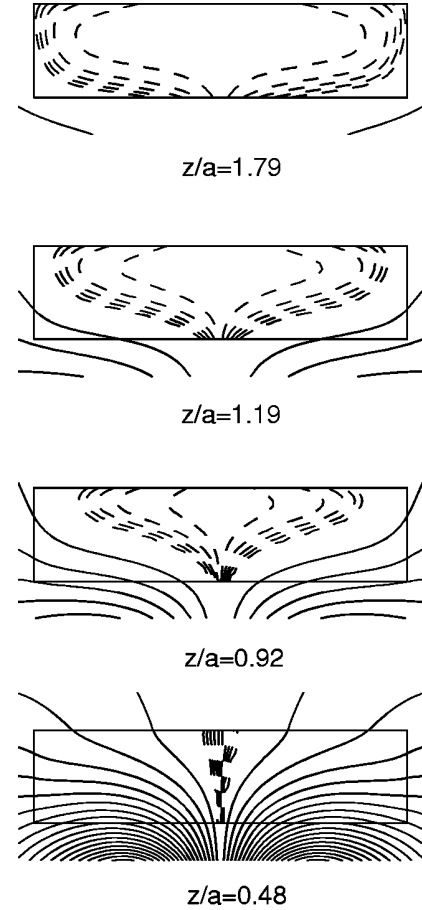


FIG. 1. Magnetic field lines when a PM approaches a superconducting disk with aspect ratio $b/a=0.25$, $\mu_0 J_c a/B_{\text{rem}}=0.1$, and creep parameter $\sigma=20$ at distances $z/a=1.79, 1.19, 0.92, 0.48$. The dashed lines are the contour lines of the current density inside the disk. The PM approaches the disk as $z(t)=z_{00}+z_0-z_0 \sin(\omega t)$, from the initial distance $z=z_{00}+z_0$ (at $\omega t=0$) to the minimum distance z_{00} (at $\omega t=\pi/2$), with a frequency of $\omega=0.1$.

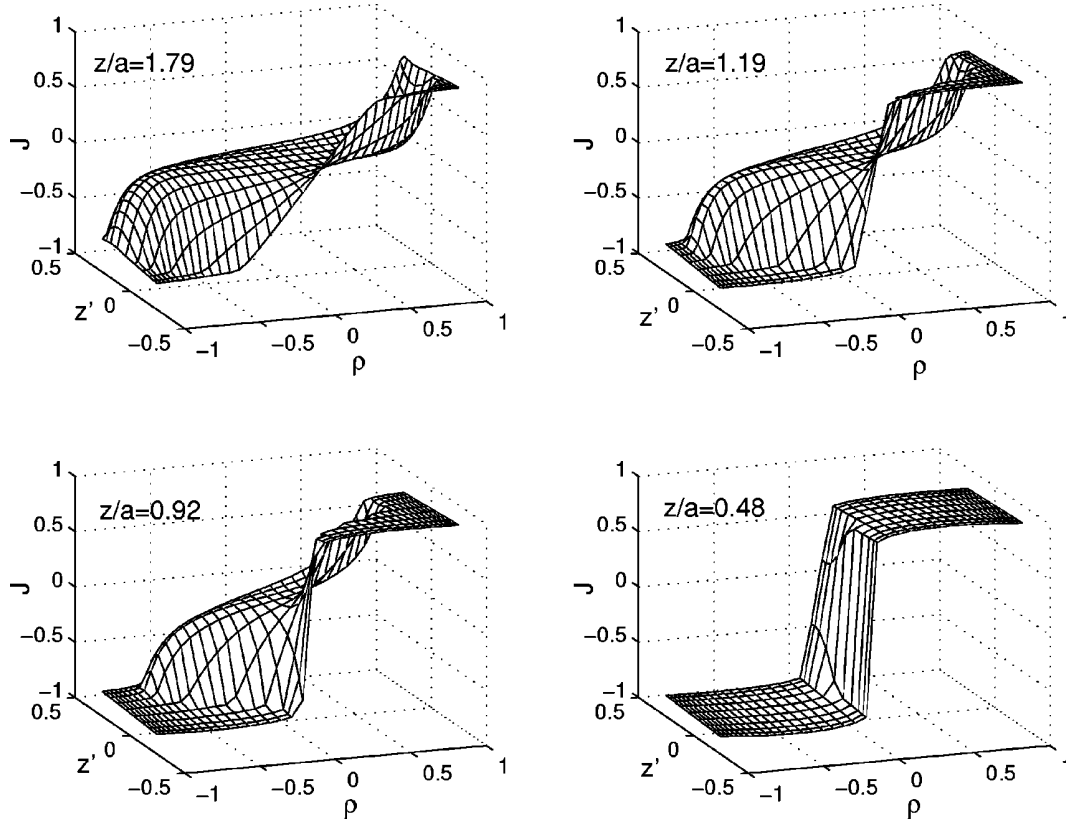


FIG. 2. Current profiles $J(\rho, z)$ for the same disk as in Fig. 1. Here $-b \leq z' \leq b$ indicates the thickness of the HTS along the z axis.

minor force loop is reversible, but beyond a certain δz , hysteretic behavior in the minor force loop will be observed. The stiffness at different distance z can then be derived as $K_z = -\partial F_z / \partial z$.

III. RESULTS AND DISCUSSIONS

A. Current and field profiles in the HTS

Figure 1 shows the magnetic flux lines (solid lines) and contours of the current density (dashed lines) when a permanent magnet is approaching a superconducting disk. Here the disk has radius a (our unit length), side ratio $b/a=0.25$, creep parameter $\sigma=20$, and critical current density $\mu_0 J_c a / B_{\text{rem}}=0.1$. The PM is a cylinder of radius $R_{\text{PM}}=0.5a$ and thickness $t_{\text{PM}}=0.25a$ with remanent induction B_{rem} . The distance between the closest flat surfaces of the HTS disk and the magnet is $z/a=1.79, 1.19, 0.92$, and 0.48 . Thus Fig. 1 visualizes the penetration of the nonuniform magnetic field of the PM into the superconducting disk. Some features different from those of the superconducting disk in a uniform magnetic field⁴⁰ can be clearly seen. Because the magnetic field is stronger at the bottom of the disk (see $z/a=0.48$ of Fig. 1), the penetration starts from the bottom of the disk, while the top surface is not penetrated. The resulting magnetic field fronts inside the disk form an onion shape rather than the symmetrical lens shape observed for homogeneous applied field. One can clearly see how the magnetic field lifts the superconductor.

Figure 2 shows the profiles of the current density $J(\rho, z)$ corresponding to Fig. 1. The current density first saturates at the edges of the bottom surface, while the current density at the edges of the top surface is smaller ($z/a=1.79$). As the PM is moving closer, the saturation spreads both into the top surface and into the middle of the disk ($z/a=1.19$ and $z/a=0.92$), until it is saturated everywhere inside the disk ($z/a=0.48$). Because we choose $\sigma=20$ (or $n=21$), the maximum current density is considerably smaller than the critical current density J_c . Increasing σ will result in a larger current density closer to J_c .

The magnetic field lines when the PM is moving away from the superconducting disk with side ratio $b/a=0.25$ and $\sigma=20$, $\mu_0 J_c a / B_{\text{rem}}=0.1$ are shown in Fig. 3 as solid lines at distances $z/a=0.12, 0.20, 0.32$, and 0.48 . The dashed lines are the contour lines of the current density inside the disk. Figure 4 shows the corresponding profiles of the current density $J(\rho, z)$. As the magnetic field is decreased, the current density is reversed inside the disk. Interestingly, the reversion begins at the bottom surface with $\rho/a = \pm 0.5$, where the magnetic field is strongest. As the PM is moving further away, the reversion spreads onto the top surface and middle of the disk (Fig. 4, $z/a=0.20$ and $z/a=0.32$), until the current is completely reversed ($z/a > 0.48$). Note that for a superconducting disk immersed in a uniform magnetic field, the reversion usually begins at the edge of the disk and spreads into the center of the sample. As the levitation force is determined by the current density $J(\rho, z)$ and by the mag-

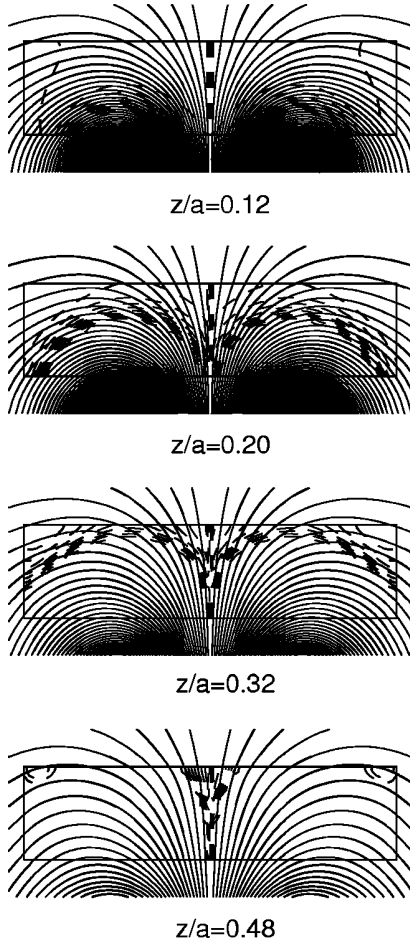


FIG. 3. Magnetic field lines when a PM is moving away from a superconducting disk with $b/a=0.25$, $\mu_0 J_c a/B_{\text{rem}}=0.1$, and $\sigma=20$ at distances $z/a=0.12, 0.20, 0.32, 0.48$. The dashed lines are the contour lines of the current density inside the disk. After approaching (not shown here) the PM recedes from the disk as $z(t)=z_{00}+z_0-z_0 \sin(\omega t)$ from the minimum distance $z=z_{00}$ (at $\omega t=\pi/2$) to the maximum distance $z=z_{00}+z_0$ (at $\omega t=\pi$), with a frequency of $\omega=0.1$.

netic field shown in Fig. 1 to Fig. 4, the features shown in these figures will be reflected in the levitation force, as will be discussed in the following.

The magnetic field lines and the profiles of the current density $J(\rho, z)$ depend on the side ratio b/a , creep exponent σ , and critical current density J_c of the superconducting disk, as well as on the dimensions and B_{rem} of the PM. Detailed results will be presented elsewhere.

B. Effect of specimen shape on F_z

As we use reduced units $a=1$ in this calculation, the effect of the shape of the HTS on the levitation is demonstrated by calculating the levitation force for different thicknesses $2b$ of the superconducting disk. The results are shown in Fig. 5(a), where $F_z(z)$ curves at $\sigma=2$, $\omega=0.1$, and $\mu_0 J_c a/B_{\text{rem}}=0.1$ are plotted for different thicknesses $2b$. The $F_z(z)$ curves show typical hysteretic behavior. For larger side ratios

b/a , the hysteretic loop is asymmetrical, with the maximum repulsive force larger than the maximum attractive force. However, as the side ratio is decreased, the hysteretic force loop becomes more and more symmetrical. For $b/a=0.05$, the curve is completely symmetric. Experimentally, symmetrical $F_z(z)$ curves have been observed in YBCO thin films,¹⁷ while in MTG bulk samples, the $F_z(z)$ curves are usually asymmetric. The reason for this is easy to understand: For a thin sample, the magnetic moment is saturated when the PM is close to the sample. When the PM is moving away from the sample, only a little decrease in the applied field saturates the magnetic moment in the reverse direction; this results in a symmetrical magnetization hysteresis loop [see Fig. 5(b), where the magnetization hysteresis loops corresponding to Fig. 5(a) are plotted], and therefore a symmetrical force loop. While for a bulk sample the magnetic moment saturates when the PM is close to the sample, it is never saturated in the reverse direction when the PM is moving far away from the disk [see the magnetization hysteresis loops for $b/a \geq 0.8$ in Fig. 5(b)], resulting in an asymmetric hysteresis loop of the magnetization and therefore an asymmetric loop of the force versus distance.

Another interesting feature shown in Fig. 5 is that a maximum is found in the repulsive force when the PM is at some distance away from the HTS, rather than at the minimum distance. Experimentally this maximum has been observed in thin films,¹⁷ while it was hardly observed in MTG samples. Riise *et al.* accredited this maximum to the dimensions of the PM, which tends to vanish with larger t_{PM} and smaller R_{PM} . And the disappearance of the maximum in MTG samples was explained by noting that bulk samples are less sensitive to a nonuniform field than films.¹⁷ Another explanation comes from Sanchez and Navau,³³ who claimed that this maximum is a result of the minimum in the derivative of the field produced by the PM, based on a constant-field-gradient model.³¹ They concluded that the maximum depends crucially on the side ratio b/a , the larger the side ratio b/a , the closer the maximum shifts to zero PM-HTS separation. When b/a is sufficiently large, the maximum may not exist. However, as can be seen from Fig. 5(a), the maximum is independent of the side ratio b/a . The peaks are observed to be at the same distance for all side ratios and even for $b \geq a$ not shown here. In a separate calculation, we have found that this maximum is independent of the dimensions of the PM. We conclude that the peak arises from the intrinsic properties of the HTS. As will be seen from figures below, the maximum depends on the creep exponent σ . The larger σ , the closer the maximum shifts to zero PM-HTS separation. When σ is sufficiently large, the maximum may not be observed any more.

Because $\sigma=n-1$, and n can be related to the depinning barrier U_0 of the sample as $n=U_0(T, B)/k_B T$,^{40,41} a smaller σ means a lower activation barrier or higher temperature. Both MTG YBCO and YBCO thin film have a relatively high pinning potential, however, experimentally when a PM approaches a thin film, it may increase the local temperature on the film, resulting in a lower σ , and therefore in a maximum. On the other hand, although the PM may increase the temperature of the surface of the bulk sample, the currents

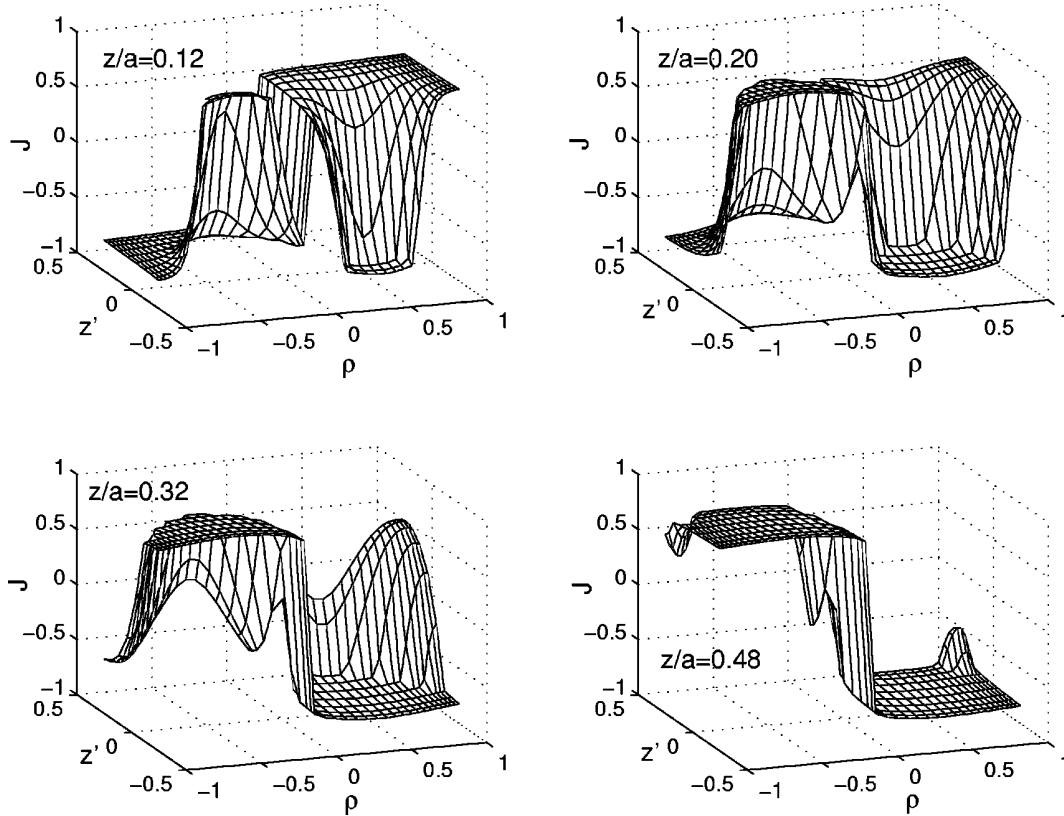


FIG. 4. Current profiles $J(\rho, z)$ for the same disk as in Fig. 3. Here $-b \leq z' \leq b$ indicates the thickness of the HTS along the z axis.

flow in a much larger volume, and the levitation force is determined by the bulk properties, so the maximum may not be observed in MTG bulk samples.

In the inset of Fig. 5(a), we show the maximum repulsive force as a function of the side ratio b/a . It can be seen from the figure that for small side ratio b/a , the maximum repulsive force increases linearly with b/a , but saturates as b/a is further increased. Technically, a superconducting disk with diameter $2a$ approximately equal to the thickness may be optimum for magnetic levitation, since further increase of the thickness will not enhance the levitation force. This calculated result is consistent with the experimental observations.²⁵

C. Effects of material properties on F_z

The properties of the HTS in our calculation are represented by two essential parameters. One is the creep exponent σ related to the depinning barrier by $n = \sigma + 1 = U_0(T, H)/k_B T$; another parameter is the critical current density J_c representing the pinning strength. The effect of σ on the magnetic levitation force is shown in Fig. 6(a), where the vertical magnetic levitation force F_z is plotted versus the distance z at $b/a = 1.4$, $\omega = 0.1$, and $\mu_0 J_c a / B_{rem} = 0.1$ for different σ values. It can be seen from Fig. 6(a) that as σ is increased, the hysteretic force loop increases and the maximum repulsive force shifts to a smaller PM-HTS separation. When σ is sufficiently large, the peak is not observed, as

discussed in the above section (the maximum at $\sigma = 100$ corresponds to minimum HM-HTS separation). On the contrary, the maximum in the attractive force shifts to larger PM-HTS separation with increasing σ . The maximum attractive force increases with σ , however, when σ is larger than 5, it decreases again and saturates at higher σ . As opposed to this, the maximum repulsive force increases monotonically with σ and reaches a saturation value at large σ , as shown in the inset of Fig. 6(a).

Figure 6(b) shows the corresponding magnetization hysteresis loops. For $\sigma = 1$, the depinning barrier is very small. Because of the relaxation effects, the applied magnetic field can penetrate deeper into the sample, similar to the case of small side ratio b/a shown in Fig. 5. The magnetization hysteresis loop and therefore the force loop are symmetric. Increasing the depinning barrier (larger σ) results in larger hysteresis loops of the magnetization. However, further increase of σ leads to a reversible response and to a smaller magnetization hysteresis loop. Interestingly, the peak in the maximum attractive force corresponds to the maximum hysteresis of the magnetization (here $\sigma = 5$) as can be seen from Fig. 6.

The sharp decrease of the levitation force from repulsive to attractive results from the nonuniform magnetic field generated by the PM and from the relaxation of the current in the HTS. According to Eq. (11), the vertical levitation force is determined by the radial magnetic field of the PM and the current density of the HTS. The radial magnetic field is

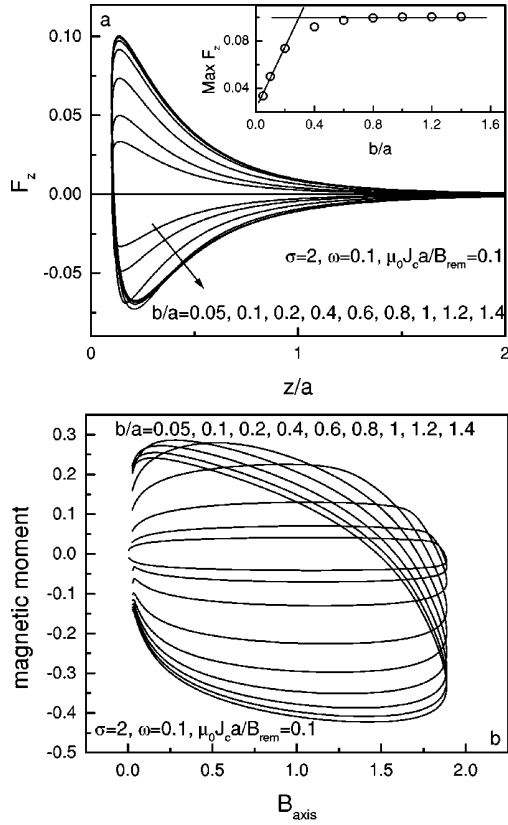


FIG. 5. (a) The vertical magnetic levitation force F_z (in units $0.01B_{rem}^2 a^2 / \mu_0$) versus the distance z at $\sigma=2$, $\omega=0.1$, and $\mu_0 J_c a / B_{rem} = 0.1$ for different thicknesses of the superconducting disk. The inset shows the maximum repulsive force as a function of the thickness; the solid lines are a guide for the eyes. (b) The corresponding magnetization hysteresis loops.

strongest close to $\rho/a = \pm R_{PM}$ at the bottom of the disk [see Eq. (2)]. Therefore, the radial magnetic field and the current close to $\rho/a = \pm R_{PM}$ on the bottom of the disk contribute more to the levitation force. When the applied field is decreased by a small amount, the current close to $\rho/a = \pm R_{PM}$ on the bottom of the disk is reversed to positive first. Although the total current is still negative (the magnetic moment is negative), the levitation force decreases sharply to a negative value, because the attractive force that results from the current close to $\rho/a = \pm R_{PM}$ at the bottom of the disk is much larger than the repulsive force resulting from the negative current in the HTS. For a small σ , because of relaxation, the current is small, and even a small decrease in the applied magnetic field may lead to complete reversal of the current, see Fig. 6; therefore the maximum attractive force occurs closer to zero PM-HTS separation. When σ is increased, the current is larger, and further decrease of the applied magnetic field is needed to reverse the current. Therefore, the maximum attractive force is larger and shifts to larger PM-HTS separations. Further increasing σ shifts the maximum attractive force to larger PM-HTS separation, but the maximum attractive force is smaller. This is because much more decrease of the applied magnetic field is needed

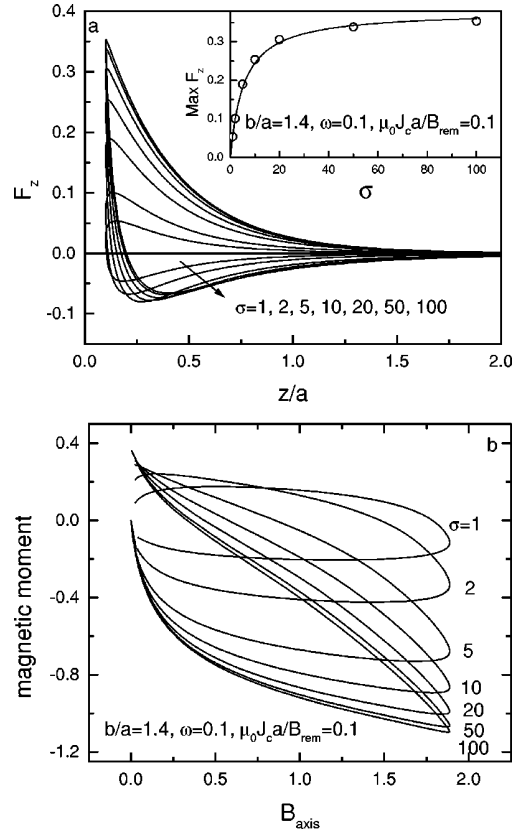


FIG. 6. (a) The vertical magnetic levitation force F_z (in units $0.01B_{rem}^2 a^2 / \mu_0$) versus the distance z at $b/a=1.4$, $\omega=0.1$ and $\mu_0 J_c a / B_{rem} = 0.1$ for various creep parameters of the superconducting disk. The inset shows the maximum repulsive force as a function of σ ; the solid line is a guide for the eyes. (b) The corresponding magnetization hysteresis loops.

to reverse the larger current when σ is increased. Although the current is larger, the radial field is smaller, resulting in the smaller maximum attractive force observed in Fig. 6(a).

Another characteristics of the HTS which drastically influences the magnetic levitation force is the critical current density. The calculated results of $F_z(z)$ at $b/a=1.4$, $\sigma=20$ and $\omega=0.1$ for different critical current densities J_c are plotted in Fig. 7(a). The corresponding magnetization hysteresis loops are shown in Fig. 7(b). For small critical current densities ($\mu_0 J_c a / B_{rem} \leq 1$), the calculated results are typical $F_z(z)$ loops, exhibiting both a repulsive force branch and an attractive force branch. The attractive force branches of the curves are hardly visible in Fig. 7(b) due to the large vertical scale. When $\mu_0 J_c a / B_{rem}$ is larger than 2, no attractive force is observed. When $\mu_0 J_c a / B_{rem}$ is larger than 6, the $F_z(z)$ curves are almost reversible ($\sigma=80,100$). This result can also be seen from the magnetization hysteresis loops shown in Fig. 7(b). Namely, increasing the critical current density leads to larger hysteresis loops and to almost reversible minor magnetization loops, since the flux lines at small changes of the applied field will not move. Experimentally, $F_z(z)$ curves with very small hysteresis width have been observed in a MTG sample,¹² indicating a very high critical current density in this sample.

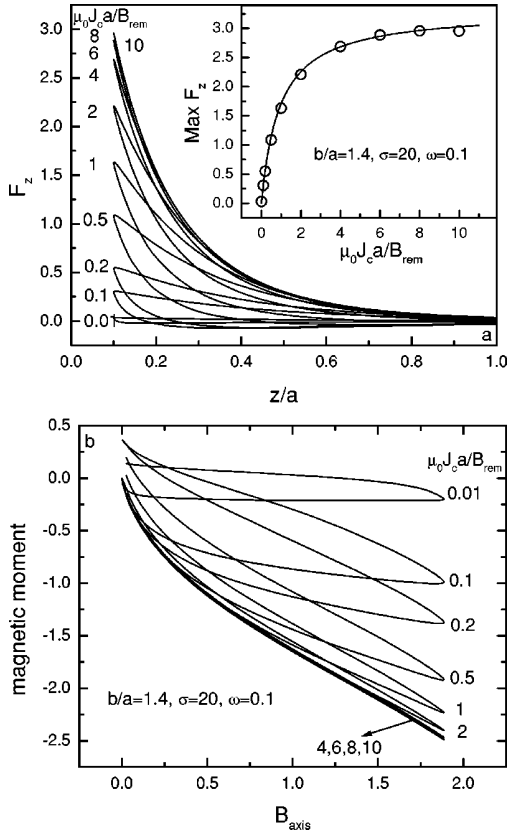


FIG. 7. (a) The vertical magnetic levitation force F_z (in units $0.01B_{rem}^2 a^2 / \mu_0$) versus the distance z at $b/a=1.4$, $\sigma=20$ and $\omega=0.1$ for different critical current densities of the superconducting disk. The inset shows the the maximum repulsive force as a function of J_c ; the solid line shows the fit $F_z = 3.31(\mu_0 J_c a / B_{rem}) / [0.93 + (\mu_0 J_c a / B_{rem})]$. (b) The corresponding magnetization hysteresis loops.

Based on the critical state model, the constant-field-gradient model³³ predicted that the maximum repulsive force F_z^{\max} depends linearly on the critical current density. In order to study this dependence, we plot in the inset of Fig. 7(a) the dependence of the maximum repulsive force as a function of the critical current density shown as open circles. It is obvious that the dependence is a nonlinear function. The linear dependence is observed only at very low critical current density $\mu_0 J_c a / B_{rem} < 0.5$. A fitting to the obtained data results in the dependence

$$F_z^{\max} = \frac{3.31(\mu_0 J_c a / B_{rem})}{0.93 + (\mu_0 J_c a / B_{rem})} \quad (14)$$

(in units $0.01B_{rem}^2 a^2 / \mu_0$) shown as a solid line in the inset. From Eq. (14) we can see that the maximum repulsive force saturates at high critical current density J_c . This saturation obviously corresponds to the case of ideal magnetic screening, which will not be enhanced by further increasing J_c .

Experimentally it is very difficult to get systematic results as shown in Figs. 6 and 7. However, Figs. 6 and 7 can be used as a quick reference for testing the properties of the

sample under investigation. By comparing the experimental results with Figs. 6 and 7, one may get an idea about the depinning barrier and critical current of the sample.

D. Force creep

It has been well known that the current density in HTS experiences relaxation (decay with time), which has been extensively studied both theoretically and experimentally in terms of the magnetization. Because the vertical magnetic levitation force is determined by the current density in the HTS and radial magnetic field generated by the PM, it is expected that the levitation force may exhibit relaxation, resulting in a time dependent levitation force in experiments. However, reports on this dynamic behavior are very few.^{24,44} On the other hand, no models so far have taken this relaxation behavior of the magnetic levitation force into account. This is quite surprising considering the operating temperature of the levitation system between a HTS and a PM, which is normally at the relatively high temperature of 77 K, where the relaxation rate is usually quite high. It is also surprising if one considers the effects of the force decay on the design of any practical applications invoking PM-HTS levitation.

In this calculation, the force relaxation is taken into account by using a voltage-current law $E(J) = E_c (J/J_c)^n$. With $1 < n < \infty$, this realistic material law describes the flux creep in terms of the magnetization inside the superconducting disk. In Fig. 8 we show the curves $F_z(z)$ at $b/a=1.4$, $\sigma=2$ and $\mu_0 J_c a / B_{rem} = 0.1$ for different frequencies ω at which the PM approaches and recedes from the HTS. It is obvious that the levitation force depends on the speed at which the PM approaches and recedes from the HTS; namely, larger speed leads to a larger force loop. As opposed to this, previous models based on the critical state model assumed that the levitation force is independent of the speed at which the PM approaches and recedes from the HTS.¹²

In the inset of Fig. 8(a), we show the maximum repulsive force as a function of the time $t = 1/\omega$ as open circles in a double logarithmic plot. The linear dependence is obvious. Fitting to the data gives a $F_z \propto t^{-m}$ dependence of F_z on time. This result actually arises from the thermally activated flux motion in the HTS, because the voltage-current law $E(J) = E_c (J/J_c)^n$ follows for a logarithmic current dependence of the activation energy $U(J) = U_0 \ln(J_c/J)$, inserted into the Arrhenius law $E = Bv = Bv_0 \exp[-U(J)/k_B T]$ (v is the vortex velocity). With this activation energy, the relaxation of the current density can be derived as $J \propto t^{-m}$ with $m = 1/\sigma$,⁴⁵ leading to the force relaxation shown in the inset of Fig. 8(a). Experimentally, the force creep has been observed to be logarithmic in time²⁴ (corresponding to the limit $m \rightarrow 0$ or $\sigma \rightarrow \infty$) within a narrow time window. It is expected that a nonlogarithmic force creep $F_z \propto t^{-m}$ will be observed if an extended time window is measured.

The force relaxation also can be clearly seen from Fig. 8(b), where the magnetization hysteresis loops corresponding to Fig. 8a are plotted. The width of the magnetization hysteresis loops increases with increasing frequency. This be-

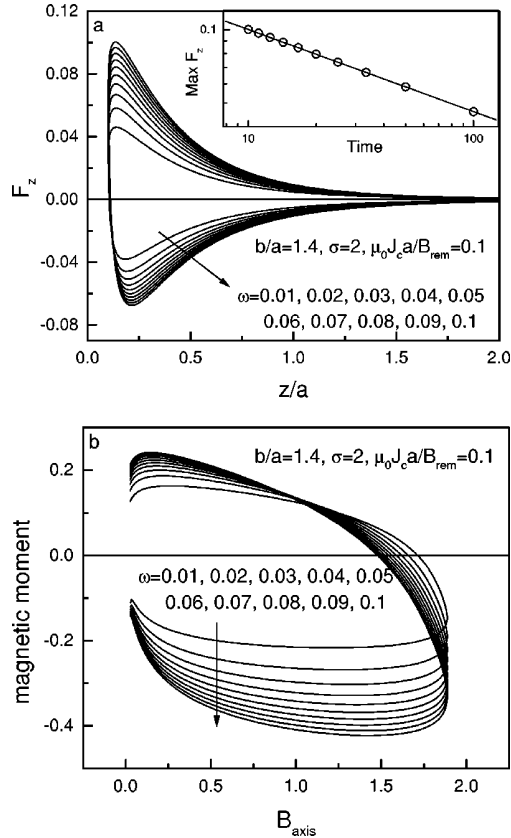


FIG. 8. (a) The vertical magnetic levitation force F_z (in units $0.01B_{rem}^2 a^2 / \mu_0$) versus the distance z at $b/a=1.4$, $\sigma=2$, and $\mu_0 J_c a / B_{rem} = 0.1$ for various frequencies at which the PM approaches and recedes from the HTS. The inset shows the relaxation of the levitation force. (b) The corresponding magnetization hysteresis loops.

havior is similar to what is observed in so-called dynamic magnetic moment experiments, in which dc magnetization hysteresis loops are measured at different sweep rates. The width of the magnetization hysteresis loop increases with increasing sweep rate. It has been proven that measurements of the dynamic magnetic moment are equivalent to the normal relaxation measurements, in which the magnetic moment is recorded as a function of time at fixed temperature and magnetic field, when studying the relaxation of HTS.^{46,47} Therefore, by measuring the vertical levitation force F_z versus z at different frequencies with which the PM approaches and recedes away from the HTS, one can study the relaxation of the force as well as the current density in the HTS.

E. Minor force loops and magnetic stiffness

One of the most important parameters used to characterize the magnetic levitation system using a PM and an HTS, is the magnetic stiffness defined as $K_z = -\partial F_z / \partial z$, which represents the spring constant associated with the vibrational motion of a levitation system. The magnetic stiffness can be determined by measuring or computing minor force loops. Some calculated minor force loops at different PM-HTS

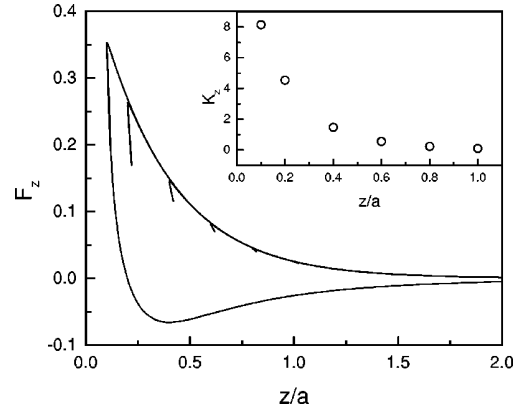


FIG. 9. The vertical magnetic levitation force F_z (in units $0.01B_{rem}^2 a^2 / \mu_0$) versus the distance z at $b/a=1.4$, $\sigma=100$, $\omega=0.1$ and $\mu_0 J_c a / B_{rem} = 0.1$. Minor force loops at different distances z are shown with a amplitude $\delta z = 0.02a$. The inset shows the stiffness of the system.

separations z are shown in Fig. 9 for $b/a=1.4$, $\sigma=100$, $\omega=0.1$, and $\mu_0 J_c a / B_{rem} = 0.1$. Here we used a small amplitude of $\delta z = 0.02a$, resulting in reversible minor force loops. Higher amplitude will lead to hysteretic behavior not shown here. The calculated vertical stiffness is plotted in the inset as a function of the PM-HTS distance z . It can be seen from Fig. 9 that one has $K_z > 0$, indicating stable levitation between a PM and a HTS. K_z decreases with increasing PM-HTS separation z . K_z may also depend on other parameters, such as J_c , ω , σ and the shapes of both the PM and the HTS. All these cases are easily computed by our numerical method. Detailed results will be presented elsewhere.

IV. CONCLUSIONS

The current density and magnetic field profiles of a superconducting disk (HTS) with radius a and thickness $2b$ immersed in the nonuniform magnetic field generated by a permanent magnet (PM) are calculated from first principles for the superconductor. From the derived current density, the magnetic levitation force between the HTS and the PM has been derived by assuming a voltage-current law $E(J) = E_c (J/J_c)^n$ and a material law $\mathbf{B} = \mu_0 \mathbf{H}$. The geometry and characteristics of the HTS drastically influence the vertical levitation force F_z . F_z depends nonlinearly on the critical current density j_c of the HTS: $F_z \approx 3.31(\mu_0 J_c a / B_{rem}) / [0.93 + (\mu_0 J_c a / B_{rem})]$. For thin samples, F_z depends linearly on the thickness of the sample, but beyond a certain thickness, F_z is nearly independent of the thickness. The flux creep also plays an important role in the magnetic levitation force, which is observed to be nonlogarithmic in time. The stiffness for the HTS and PM system has also been derived. Our calculations reproduce many of the features observed in levitation experiments.

After this work was submitted, two papers by Sanchez

and Navau^{48,49} appeared which consider the same geometry of a superconducting disk in a levitating inhomogeneous field. The transparent model of interacting coaxial superconducting rings they used can be justified by our exact method, though it is typically less accurate and treats only the static case, while our method includes the full dynamic behavior, i.e., it also yields the time and velocity dependences of the levitation force.

ACKNOWLEDGMENTS

The authors would like to thank the Australian Research Council for financial support. E.H.B. acknowledges support from the Australian Research Council, IREX Program, and the hospitality of the Institute for Superconducting and Electronic Materials, University of Wollongong. G. Li would like to thank Professor D. L. Yin for helpful discussion.

- ¹J. R. Hull, E. F. Hilton, T. M. Mulcahy, Z. J. Yang, A. Lockwood, and M. Strasik, *J. Appl. Phys.* **78**, 6833 (1995).
- ²B. R. Weinberger, L. Lynds, J. R. Hull, and U. Balachandran, *Appl. Phys. Lett.* **59**, 1132 (1991).
- ³J. M. Goodkind, *Rev. Sci. Instrum.* **70**, 4131 (1999).
- ⁴J. T. Hull, *Semicond. Sci. Technol.* **13**, R1 (2000).
- ⁵J. R. Hull, T. M. Mulcahy, K. L. Uherka, R. A. Erick, and R. G. Abboud, *Appl. Supercond.* **2**, 449 (1994).
- ⁶H. Kamenno, Y. Miyagawa, R. Takahata, and H. Ueyama, *Appl. Supercond.* **9**, 992 (1999).
- ⁷H. J. Bornemann, T. Ritter, C. Urban, O. Zaitsev, K. Weber, and H. Rietschel, *IEEE Trans. Appl. Supercond.* **2**, 439 (1994).
- ⁸Q. Y. Chen, Z. Xia, K. B. Ma, C. K. McMichael, M. Lamb, R. S. Cooley, P. C. Fowler, and W. K. Chu, *Appl. Supercond.* **9**, 457 (1994).
- ⁹T. A. Coombs, A. M. Campbell, I. Ganney, W. Lo, T. Twardowski, and B. Dawson, *Mater. Sci. Eng., B* **53**, 225 (1998).
- ¹⁰M. Tosa and A. K. Yoshida (unpublished).
- ¹¹B. Oswald, M. Krone, M. Soll, T. Stresser, J. Oswald, K. J. Best, W. Gawalak, and L. Kovalev, *IEEE Trans. Appl. Supercond.* **9**, 1201 (1999).
- ¹²J. R. Hull and A. Cansiz, *J. Appl. Phys.* **86**, 6396 (1999).
- ¹³M. Ullrich, A. Leenders, and H. C. Freyhardt, *Appl. Phys. Lett.* **68**, 2735 (1996).
- ¹⁴D. Shi, D. Qu, S. Sagar, and K. Lahiri, *Appl. Phys. Lett.* **70**, 3606 (1997).
- ¹⁵W. Hennig, D. Parks, R. Weinstein, and R. P. Sawh, *Appl. Phys. Lett.* **72**, 3059 (1998).
- ¹⁶B. Lehdorff, H. Kürschner, B. Lücke, and H. Piel, *Physica C* **247**, 280 (1995).
- ¹⁷A. B. Riise, T. H. Johansen, H. Bratsberg, M. R. Koblishka, and Y. Q. Shen, *Phys. Rev. B* **60**, 9855 (1999).
- ¹⁸P. Z. Chang, F. C. Moon, J. R. Hull, and T. M. Mulcahy, *J. Appl. Phys.* **67**, 4358 (1990).
- ¹⁹M. Murakami, *Melt Processed High-Temperature Superconductors* (World Scientific, Singapore, 1992).
- ²⁰C. P. Bean, *Phys. Rev. Lett.* **8**, 250 (1962).
- ²¹C. P. Bean, *Rev. Mod. Phys.* **36**, 31 (1964).
- ²²F. C. Moon, *Superconducting Levitation* (Wiley, New York, 1994).
- ²³Y. Yeshurun and A. P. Malozemoff, *Phys. Rev. Lett.* **60**, 2202 (1988).
- ²⁴A. B. Riise, T. H. Johansen, H. Bratsberg, and Z. J. Yang, *Appl. Phys. Lett.* **60**, 2294 (1992).
- ²⁵J. Unsworth, J. Du, B. J. Crosby, and J. C. Macfarlane, *IEEE Trans. Magn.* **29**, 108 (1993).
- ²⁶B. A. Tent, D. Qu, D. Shi, W. J. Bresser, P. Boolchand, and Z. X. Cai, *Phys. Rev. B* **58**, 11 761 (1998).
- ²⁷Z. J. Yang, *J. Supercond.* **5**, 529 (1992).
- ²⁸Z. J. Yang, *Appl. Supercond.* **2**, 559 (1994).
- ²⁹Z. J. Yang and J. R. Hull, *J. Appl. Phys.* **79**, 3318 (1996).
- ³⁰A. A. Kordyuk, *J. Appl. Phys.* **83**, 610 (1998).
- ³¹C. Navau and A. Sanchez, *Phys. Rev. B* **58**, 963 (1998).
- ³²F. Hellman, E. M. Gyorgy, D. W. J. Jr., H. M. O'Bryan, and R. C. Sherwood, *J. Appl. Phys.* **63**, 447 (1988).
- ³³A. Sanchez and C. Navau, *Physica C* **268**, 46 (1996).
- ³⁴T. Torng and Q. Y. Chen, *J. Appl. Phys.* **73**, 1198 (1992).
- ³⁵P. Schönhuber and F. C. Moon, *Appl. Supercond.* **2**, 253 (1994).
- ³⁶M. Däumling and D. C. Larbalestier, *Phys. Rev. B* **40**, 9350 (1989).
- ³⁷L. W. Conner and A. P. Malozemoff, *Phys. Rev. B* **43**, 402 (1991).
- ³⁸A. B. Riise, T. H. Johansen, and H. Bratsberg, *Physica C* **234**, 108 (1994).
- ³⁹T. H. Johansen, H. Bratsberg, A. B. Riise, H. Mestl, and A. T. Skjeltop, *Appl. Supercond.* **2**, 535 (1994).
- ⁴⁰E. H. Brandt, *Phys. Rev. B* **58**, 6506 (1998).
- ⁴¹E. H. Brandt, *Phys. Rev. B* **54**, 4246 (1996).
- ⁴²E. H. Brandt, *Phys. Rev. B* **59**, 3369 (1999).
- ⁴³E. H. Brandt, *Phys. Rev. B* **64**, 024505 (2001).
- ⁴⁴F. C. Moon, P. Z. Chang, H. Hojaji, A. Barkatt, and A. N. Thorpe, *Jpn. J. Appl. Phys.* **29**, 1257 (1990).
- ⁴⁵E. H. Brandt, *Phys. Rev. Lett.* **76**, 4030 (1996).
- ⁴⁶H. G. Schnack, R. Griessen, J. G. Lensink, C. J. van der Beek, and P. H. Kes, *Physica C* **197**, 337 (1992).
- ⁴⁷M. Jirsa, L. Pust, H. G. Schnack, and R. Griessen, *Physica C* **207**, 85 (1993).
- ⁴⁸A. Sanchez and C. Navau, *Phys. Rev. B* **64**, 214506 (2001).
- ⁴⁹C. Navau and A. Sanchez, *Phys. Rev. B* **64**, 214507 (2001).